Topographic Structure from Motion: a new development in photogrammetric measurement

Mark A. Fonstad[1], James T. Dietrich[1], Brittany C. Courville[2], Jennifer L. Jensen[2], Patrice E. Carbonneau[3]

[1]Department of Geography, University of Oregon, Eugene, OR 97403 USA
[2]Department of Geography, Texas State University, TX 78666 USA
[3]Department of Geography, Durham University, Durham UK

1. Introduction

The production of high-resolution topographic datasets is of increasing concern and application throughout the geomorphic sciences (Butler et al., 2001; Hancock and Willgoose, 2001; Lane, 2003; Bird et al., 2010; Fonstad and Marcus, 2010). A wide range of topographic measurement methods have evolved to meet this production need. Despite the range of available methods, the production of high resolution, high quality digital elevation models (DEMs) generally requires a significant investment in personnel time, hardware and/or software. Image based methods, such as digital photogrammetry (Chandler, 1999; Lane, 2000; Butler et al., 2002; Chandler et al., 2002; Baily et al., 2003; Carbonneau et al., 2003; Lane et al., 2003; Westaway et al., 2003; Gimenez et al., 2009; Marzloff and Poesen, 2009; Lane et al., 2010), have steadily been decreasing in costs. Photogrammetry is becoming accessible to a wider base of users following the development of methods allowing for the accurate calibration of non-metric cameras and the increasingly reliable automation of the photogrammetric process (*e.g.* Carbonneau et al., 2004; Chandler, 1999; Chandler et al., 2002). Recent developments should lower the cost of image based topography even further. Initially developed for the purpose of rapid, inexpensive and easy three dimensional surveys of buildings or small objects, the Structure from Motion approach (SfM) is a purely image based method that could deliver a step change if transferred to the geomorphic sciences.

While a full review of the SfM process is not appropriate for this manuscript (see Snavely et al. [2006 and 2008] for a basic overview of this computer vision process, and Snavely, [2008] for a complete description), the following gives a brief overview of the approach in a qualitative

manner. Similarly to traditional photogrammetry, SfM uses images acquired from multiple

viewpoints in order to restitute the three dimensional geometry of an object. However, SfM

diverges significantly from traditional photogrammetry in that in SfM, no ground control is

required to restitute that camera parameters (focal length, distortion and position) and the relative

topographic variations in a scene. This technology is based on progress in the area of automated

image matching. By automatically finding a very large number of conjugate image points in

several images, the colinearity equations which describe the relationship between a three

dimensional object and its projection onto a two dimensional image can be solved and

topography calculated (See Wolf and Dewitt, 2000). In the traditional photogrammetry language,

the bundle adjustment is done after coordinate system rectification using ground control points

(*i.e.* in real, object space), whereas in the SfM process bundle adjustment occurs before

coordinate system rectification (*i.e.* in image space). Only after the photogrammetric bundle

adjustment process creates a point cloud are ground control points necessary to rectify the entire

point cloud to a desired coordinate system. Another non-technical distinction to be noted is that

the SfM method can be performed entirely with freely available software packages which are

easily accessible to non-specialists.

Earlier SfM approaches in geomorphology have been previously discussed by Heimsath and

Farid (2002, 2003). However, it should be noted that in recent years, the SfM workflow has

been significantly improved and that current SfM software operates with a significantly higher

level of automation. Additionally, some of the problematic assumptions in this earlier use of

SfM (and noted by Chandler et al., 2003) have since been removed. When the number of photos

of the same areas is quite large, modern SfM algorithms appear to have the same level of

robustness as traditional photogrammetry. This reduces the camera backcalculation errors per picture. Most importantly, however, has been the rise of standalone, freely-available, and easy-to-use SfM software, designed for general computer users. The progress in the refining of these tools over the past two or three years has been stunning, and it seems inevitable that these SfM approaches will become appropriate to an even wider range of instrument platforms. Verhoeven (2009) and Verhoeven et al. (2009) have made introductory tests of the modern SfM process using low-altitude helikites in archaeology. A handful of other recent SfM applications to topography have been presented previously at professional conferences and published in abstracts and proceedings (Dietrich, 2010; Fonstad et al., 2010; Dietrich et al., 2011; Fonstad et al., 2011a, b). Dowling et al. (2009) used SfM and a hand-held camera to study soil erosion over a 1 m^2 plot. Templeton et al. (2010) used a UAS helicopter and SfM to generate DEMs for ecohydrological research. Welty et al. (2010) used hand-held camera images taken from a plane to construct the topography of the Columbia Glacier. Whilst these SfM DEMs are remarkably easy to produce and visually stunning, the errors and limitations of this new method are not yet known. Such errors can profoundly influence uses of these DEMs in geomorphology, such as in sediment budgeting (Wheaton et al., 2010). The crucial research question we address is this: what is quality of the DEMs produced by the SfM method? First, we will demonstrate that the SfM approach can be applied in a fluvial geomorphology context in order to restitute high-resolution topography. Second, we will show that the outputs of the SfM workflow are of equal quality to those of an independently acquired airborne LiDAR validation dataset.

2. Assessment of Topographic Accuracy

2.1. Study Area

We chose to test the SfM approach using a helikite platform at Pedernales Falls State Park in Texas, USA. The Pedernales River in this park is primarily a bedrock-defined river with strong jointing that creates an abruptly alternately wide and narrow planform carved into limestone of Pennsylvanian age in the Marble Falls Limestone formation (Figure 1). The exposed bedrock channel/floodplain system is 150 meters wide, and is buffered on either side by high bluffs covered in dense Oak/Juniper forest. On the day of the fieldwork, moderately strong winds precluded us from imaging all of the channel width, so we concentrated our imagery comparisons on the south half of the channel where access was allowed by the State Park administration. The high relief of the channel is controlled by intense bedrock jointing, and associated with diverse solution weathering features, these characteristics make an ideal location to test the accuracy and precision of a terrain modeling process over a relatively small area, approximately 3.6 hectares.

2.2 Image Acquisition

Low altitude aerial photographs were collected with a compact digital camera affixed to a unique helium-filled blimp, an Allsopp Skyshot helikite[©] (Vericat et al., 2009). The helikite was released on 100 meters of control line and walked around the study area to collect photographs covering the study area. The effects of wind and movement limited the height of the helikite to an average of 40 meters, with heights reaching a maximum of 70 meters and as low as 10 meters. The camera used in this study had an effective resolution of 10 megapixels that translated to

ground resolutions of between 1 cm and 10 cm. The camera was programmed to capture 3 photographs every 10 seconds, which provided substantial overlap in sequential photographs, which is essential for the image matching algorithms used in SfM.

2.3. Global Positioning System data collection and processing

We used a Trimble GeoXH GPS unit to collect ground reference coordinates on March 26, 2011. GPS data was collected by averaging 180 real-time corrected positions per point feature. To ensure quality, the GPS was set to only collect locations with a maximum position dilution of precision (PDOP) ≤ 4 and 3D GPS mode. The data were then post-processed using the GPS Analyst extension for ArcMap to derive the best position estimate for all ground control points. This post-processing resulted in 25 ground reference points, with a planimetric positional accuracy ranging from 0.06 m to 0.08 m ($\mu=.07$ m; $\sigma = 0.007$ m) and vertical uncertainties ranging from 0.08 m – 0.16 m. Horizontal coordinates (X,Y) were referenced to UTM Zone 14N, WGS 84, while GPS Z-values were referenced to the North American Vertical Datum 1988 (NAVD88) using a Geoid03 separation for orthometric height comparison with the LiDAR data.

2.4. SfM point cloud extraction and geographic projection

The 304 photographs that provided the best coverage of the study area were selected and processed using the Photosynth desktop application. This produced a 3-dimensional reconstruction of photographs and a point cloud of features that were present in the photographs. Utilizing a third party application, SynthExport (http://synthexport.codeplex.com), the point

cloud was downloaded as a PLY (Polygon File Format) file. Preliminary editing of the raw point cloud was performed in MeshLab (http://meshlab.sourceforge.net/) to remove a small number of extraneous points that were clearly errors. The point cloud consisted of 554,308 points in an arbitrary, internally consistent Cartesian coordinate system.

Ten of the 25 GPS points were matched to spatially coincident features in the SfM point cloud. These ten points were selected based on our ability to identify the surface feature in the SfM point cloud and navigate directly to the feature in the field to record the GPS position. The ten GPS feature positions were used as ground control points to facilitate a full 3D coordinate transformation. We used the open-source software program JAG3D (http://javagraticule3d.sourceforge.net/) to perform the 3D transformation from the SfM Cartesian coordinates to GPS-observed UTM coordinates. A 7-parameter transformation was utilized to calculate a uniform scaling factor along with independent factors for rotation and translation in all three axes of the point cloud. The transformation was applied to entire point cloud resulting in root mean squared errors (RMSE) of 0.442 meters in the X direction, 0.458 meters in the Y direction, and 0.185 meters in the Z (vertical) direction. The remaining fifteen GPS points were used to test the accuracy of the transformation in the Z direction. The Z values for the fifteen validation points were compared against a natural neighbor interpolated surface created from the georeferenced SfM data using a 0.5 meter cell size. Results indicate a near 1:1 fit between SfM and GPS GCP and validation points (Figure 2).

2.5. LiDAR data collection and processing

The LiDAR data were acquired in spring and early summer of 2006 with an Optech 2050 airborne system. The data acquisition was part of a larger initiative to provide Federal Emergency Management Agency (FEMA) compliant elevation data for specific areas within the larger Capital Area Council of Governments (CAPGOG) in central Texas. Acquisitions were designed to provide a relatively high-density dataset of mass points suitable for development of contours required for hydraulic/hydrological model development, flood mitigation assessment, and environmental impact analysis.

The multiple-return datasets were delivered as .LAS files in the State Plane 4023 (Survey Feet), NAD83 and NAVD88 (U.S. Foot) coordinate systems. The point cloud density of the LiDAR data was 0.33 points/m^2. We re-projected the LiDAR data to the UTM coordinate system for our study and adjusted vertical units to meters. Additionally, since the SfM approach only provides first surface Z-values (i.e., unlike LiDAR, SfM does not detect the ground beneath vegetation unless there are canopy gaps), we used all LiDAR returns for comparisons and to generate elevation surfaces.

2.6. SfM, LiDAR, and GPS comparisons

We also compared the agreement between the SfM, GPS, and LiDAR datasets to assess relative differences between data acquisition methods. Since neither the LiDAR nor the SfM points are exactly spatially-coincident with the GPS point observations, we extracted the nearest point neighbor for each dataset (i.e., SfM and LiDAR points nearest in spatial proximity to each GPS

point were used for comparison). Results of these comparisons are provided in Table 1.

The horizontal and vertical accuracies of the SfM and LiDAR datasets were both within a reasonable level of accuracy. The relatively large difference between the LiDAR and GPS validation points is likely due to the sparse sampling density of the LiDAR acquisition (0.33 points/m^2), whereas the SfM point cloud was much more dense (10.8 points/m^2). Based on the values presented in Table 1, we believe the level of accuracy for both the LiDAR and SfM datasets was sufficient for direct comparison of SfM and LiDAR. We performed this comparison by spatially-joining the SfM features directly to the LiDAR dataset, where each LiDAR point is compared based on the SfM point closest in spatial proximity.

2.7 Results

The elevation surfaces produced from both the SfM and LiDAR datasets are presented in Figure 3. The SfM results clearly have better feature representation when compared to this specific LiDAR dataset. The SfM point density was 10.8 points/m^2 compared to 0.33 points/m^2 for the LiDAR dataset. Given the magnitude of difference in densities, a quantitative comparison of SfM Z-values relative to a LiDAR-derived elevation model would include significant interpolation in some areas where LiDAR returns were not present.

In light of these considerations, we performed comparison of SfM and LiDAR Z-values based on spatial proximity, just as we compared both dataset Z-values with the GPS validation points. This analysis approach resulted in 30,486 observations (i.e., the number of first return LiDAR

records in our study area dataset) for comparison. SfM points were spatially-joined to LiDAR points in the GIS. We then evaluated the agreement between the two datasets by subtracting LiDAR Z-values from SfM Z-values. The average distance between individual SfM and LiDAR points was 0.27 m (σ = 0.25 m).

Results of the SfM-LiDAR comparisons are presented in Figure 4. The mean difference of SfM and LiDAR Z-values within the study area was 0.60 m (+/- 1.08). Regression of SfM to LiDAR Z-values resulted in a 97% explanation of variance present in the LiDAR dataset. We acknowledge that the relationship is not 1:1 for all points within each dataset, particularly for those points outside elevation range of our training dataset (250 m – 259.2 m). It is just beyond the upper limit of our calibration data that the 1:1 line begins to deviate from the regression line, though the deviation is relatively small.

A map of the error distribution between the two datasets is provided in Figure 5. Inspection of Figure 5 provides an opportunity to assess spatially the accuracy of the SfM approach relative to LiDAR. Of particular note is the light area at the south-western section of the study area. This area is comprised of topographically-varying features such as trees, large boulders, and sand. Further, the SfM point-cloud density is lower for this region of our study area as our research objectives were focused deriving an accurate bare-earth model.

3. Discussion

Structure from motion is appealing as a method because reduced calibration and geometric needs allows both off-the-shelf and archival camera systems to be potential data sources. We suspect that traditional photogrammetry would have similar accuracy results to our own, assuming that it could be accomplished from a similarly close-range platform as our helikite system. However, Rango et al. (2009) found that unconstrained imagery acquired from a powered Unmanned Airborne System (UAS) was difficult to use in standard photogrammetry packages. These authors found that an additional step was needed which involved external image mosaicking software based on the same image matching techniques used in SfM. This would therefore suggest that an increased use of image matching technology is required in the production of topography from imagery either with traditional photogrammetry or SfM approaches.

For the purposes of mapping topography from a low-altitude platform acquiring non-metric imagery, we have found that SfM can generate aerial LiDAR-like accuracy and precision or better (roughly one point per square decimeter) for a non-vegetated surface (Figures 6 and 7). Under ideal flying conditions, a wide range of instrument heights, and high-contrast topographic surfaces, our extracted point clouds have densities closer to lower-resolution Terrestrial Laser Scanning (TLS) than to aerial LiDAR, with some point clouds approaching one point per square centimeter, particularly with new dense point cloud SfM software. For many applications, the slightly lower spatial resolution of the current helikite-generated points may outweigh the tremendous cost of TLS systems. The acquisition of a TLS is two or three orders of magnitude more expensive than the helikite system. A traditional ground survey using a total station would be of similar cost to the helikite system, but the resulting topographic point density would be orders of magnitude less than that we were able to collect in a couple of hours using the SfM approach.

The SfM approach has some drawbacks. As the image matching algorithm relies on image texture, areas of low textural diversity will yield poor point clouds. This could include areas of bare sand, snow, or other highly flat surfaces. Objects with different coloration and textures at different orientations, such as highly reflective surfaces, will likewise produce poor point clouds. In our study area, deep water absorbs and scatters light, reducing textural detail and yielding lower point densities. The SfM approach requires several images for any given point in order to both compute its location in the point cloud and to backcalculate camera parameters. How many pictures? The simple answer is: the more the better. We recommend a minimum of five or ten pictures, but areas with greater than these numbers (especially areas with subtle topography) should yield better digital topography. Also, the texture-based basis of the automated image matching means that a scale of imagery is needed that captures high detail. If the camera is too far away to make out a small bedrock step, or individual tree leaves, it will not have the textural features required to accurately calculate a point cloud in that area. This probably means that SfM is most effective in small study areas, where moderate-quality cameras have enough resolution to capture detailed texture and are also light enough to go on UAVs, the tops of poles, or other hand-controlled platforms. Large area mapping with SfM would require both a platform that could easily move long distances and yet at the same time take very high-resolution imagery with little or no motion blur. We also recommend imagery at more than one distance from the topography if possible. Imagery from a further distance helps to reduce systematic distortions over large distances, whereas close-in imagery produces the fine-detail point clouds.

Improvements can definitely be made to the helikite/SfM system used in this first test. The Microsoft Photosynth software we used to extract topography performs what is known as "sparse bundle adjustment". The 3D point density is fairly low, as the primary aim of Photosynth is to rectify imagery, not reconstruct 3D surfaces. A much richer point density can be extracted using advanced software. PMVS2 (freely available online), as one example, can take output data from Photosynth, as well as the original images, and can increase the number of points by ten or twenty times. We chose not to perform this more advanced reconstruction for this paper, as our intention was to highlight the results from the very simple Photosynth process. Advanced PMVS2 reconstruction, however, likely would have increased point densities comparable to many TLS systems. The danger in increasing point densities and/or increasing the spatial area is that the number of images and points used in the bundle adjustment may overwhelm Photosynth which was not originally designed for this type of use. An alternative approach would be to break the images and matched points into sections for bundle adjustment, and then remerge these sections together. This might be done using a different software system. Instead of Photosynth, Noah Snavely's Bundler software can perform a sparse bundle adjustment similar to Photosynth, but the outputs of Bundler can be split into more manageable sections using a package known as CMVS, and results from this software can then be densified in PMVS. A recent software product, Autodesk123D Catch, incorporates many of these options into a straightforward interface. All of these software packages are available online for free. The advantage of using this more complex software system would be the ability to manage the reconstruction of very large areas at high point density by distributing the bundle adjustment into many individual chunks that could individually be managed by standard desktop computers.

Another possible extension to the SfM topographic reconstruction is the automatic orthorectification of the original images. Photosynth calculates camera parameters (such as camera location and direction). While these parameters are in the same initial relative coordinate system as is the topographic point cloud, they could, in principle, be transformed to an absolute coordinate system along with the point cloud. After the point cloud has been converted to a DEM, the camera parameters could then be used to project the original images onto the DEM. As the DEM was made directly from these images, the orthorectification should be of extremely high quality. The recently released (but not free) software package Agisoft Photoscan uses a SfM process similar to Bundler than both creates dense point clouds and orthorectifies the individual images. Another option would be to replace the ground control points collected using ground-based GPS with a GPS associated with the camera(s) used. As the camera parameters are calculated along with the point cloud, the transformation from a relative to an absolute coordinate system could use these platform based GCPs rather than ground GCPs; such was the approach of Welty et al. (2010), and it is one of the options in Photoscan. The disadvantage of this approach is that some platforms (helikites, UAVs) are not able to carry large differential GPS systems, so the positional accuracy of the GPS becomes a potential issue. A third extension to our approach is the possible use of a high-definition (HD) videocamera rather than using individual camera frames taken at some time interval. While HD videocameras are of lower resolution than individual camera frames, the fact that many more images are being captured means that there is far more overlap between images. Faster-moving platforms such as fixed-wing UAVs (Dunford et al., 2009) or low-flying aircraft might be able to use HD cameras to deal with the multiple-frame overlap required by the SfM process. If viable, this approach would

allow already-existing aerial video footage to be converted to three-dimensional landscapes given the right conditions.

While a complete cost-benefit analysis of the SfM approach compared with other topography data collection approaches is beyond the scope of this study, some potential uses are immediately evident. Very small area, fine resolution topographic studies would benefit from the SfM approach immediately. Such applications might include fluvial features such as gravel river bed particle analysis, bar and bank forms, woody debris geometry, and small- and medium-sized channel 3D morphology. Many of these studies could be accomplished with simple hand-held cameras. The introduction of higher platforms, such as the helikite, allows a much larger number of topographic features to be measured. Rather than expensive platforms, another option is to have many people taking images with several cameras. This "flash mob" approach seems like a reasonable tactic for extracting 3D environments over small areas in a short amount of time. Disaster response (floods, hurricanes, debris flows), for example, would be helped by having high-resolution 3D data quickly. Sending out a group determined to take large numbers of pictures of the area with many cameras should produce useful SfM-derived data at very low cost. Larger projects over larger areas may require alternative approaches to SfM, but this study should be helpful in determining some of the cost-benefit information needed to make that decision.

The ease of use and wide applicability of the SfM software raises some interesting possibilities. It may be possible to extract useful 3D topography from motion pictures and video products. While these are usually of lower resolution than individual photos, they have the advantage of

consistent lighting, many overlapping frames and images, and a long history. Some "impossible" geomorphic measurements, such as the precise measurement of woody debris over large and difficult to access areas, may be well-served by SfM. Our testing of SfM from a low-altitude instrument platform found the technique to be extremely simple-to-use, and had high topographic quality and precision, at least in areas with "complex" surfaces. Further tests of this approach in other environments and with different platforms would be very useful to geomorphology as a whole; there are environments where this technique may be failure-prone, for example, "smooth" surfaces such as uniform snow and sand may be very difficult surfaces from which to extract SfM topographic datasets. Nevertheless, these tests could be completed at essentially no cost but sweat equity, and further software development may improve the SfM approach even further.

4. Conclusions

We tested the utility of the Structure from Motion photogrammetric approach in a bedrock fluvial setting using a helikite platform, and found it to be of high accuracy and precision, even when compared to aerial LiDAR data. Remote sensing in many parts of geomorphology would greatly benefit from approaches like SfM that take low cost images and convert them, with little or no technical training and free software, to high quality topographic datasets. The approach is straightforward, and takes very little time for raw data collection and data processing. Recent advances in software power and usability should allow exactly that, provided the resulting topographic datasets are of high quality. Moreover, the potential exists to apply this approach to historic, archival, and nonstandard imagery sources such as motion pictures, and to extend

photogrammetry to a larger number of platforms such as very small UAVs and groups of individuals with their own cameras.

Acknowledgements

.

REFERENCES

Baily, B, Collier P, Farres P, Inkpen R, Pearson A. 2003. Comparative assessment of analytical and digital photogrammetric methods in the construction of DEMs of geomorphological forms. *Earth Surface Processes and Landforms* **28**(3): 307-320.

Bird S, Hogan, D, Schwab, J. 2010. Photogrammetric monitoring of small streams under a riparian forest canopy. *Earth Surface Processes and Landforms* **35**(8), 952-970.

Butler JB, Lane SN, Chandler JH. 2001. Characterization of the structure of river-bed gravels using two-dimensional fractal analysis. *Mathematical Geology* **33**(3): 301-330.

Butler JB, Lane SN, Chandler JH, Porfiri E. 2002. Through-water close range digital photogrammetry in flume and field environments. *Photogrammetric Record* **17**(99): 419-439.

Carbonneau PE, Lane SN, Bergeron NE. 2003. Cost-effective non-metric digital photogrammetry and its application to a study of coarse gravel surfaces. *International Journal of Remote Sensing* **24**(14): 2837 - 2854.

Chandler J. 1999. Effective application of automated digital photogrammetry for geomorphological research. *Earth Surface Processes and Landforms* **24**(1): 51-63.

Chandler J, Ashmore P, Paola C, Gooch M, Varkaris F. 2002. Monitoring river-channel change using terrestrial oblique digital imagery and automated digital photogrammetry. *Annals of the Association of American Geographers* **92**(4): 631-644.

Chandler JH, Mills JP, Robson S, Lane SN. 2003. Comment on "Hillslope topography from unconstrained photographs" by A.M. Heimsath and Hany Farid. *Mathematical Geology* **35**(3): 347-350.

Dietrich JT. 2010. Visualizing small-scale geomorphic features using 3D models derived from Microsoft Photosynth. Poster presentation, 41st Binghamton Geomorphology Symposium, Columbia, SC, USA 15-17 October, 2010.

Dietrich JT, Fonstad MA, Courville BC, Jensen JL, Carbonneau PE. 2011. High resolution, automated, low-cost topographic mapping with Microsoft Photosynth. Paper presentation, Annual Meeting of the Association of American Geographers, Seattle, WA, USA, 12 April, 2011.

Dowling TI, Read AM, Gallant JC. 2009. Very high resolution DEM acquisition at lost cost using a digital camera and free software. 18th World IMACS / MODSIM Congress, Cairns, Australia 13-17 July 2009. 2479 – 2485.

Dunford R, Michel K, Gagnage M, Piegay H, Tremelo ML. 2009. Potential and constraints of unmanned aerial vehicle technology for characterization of Mediterranean riparian forest. *International Journal of Remote Sensing* **30**(19): 4915-4935.

Fonstad MA, Dietrich JT, Courville BC, Jensen JL. 2011. Lighter-than-air blimps as a testbed for river remote sensing techniques. Poster presentation, Annual Meeting of the American Geophysical Union, San Francisco, CA, USA, 16 December, 2010.

Fonstad MA, Dietrich JT, Courville BC, Jensen JL., Carbonneau PE. 2011a. High resolution, low-cost 3D riverscape mapping using field photography. Paper presentation, Annual Meeting of the American Fisheries Society, Seattle, WA, USA, 8 September, 2011.

Fonstad MA, Dietrich JT, Courville BC, Jensen JL, Carbonneau, PE. 2011b. Topographic

Structure from Motion. Paper presentation, Annual Meeting of the American Geophysical Union,

San Francisco, CA, USA, 9 December, 2011.

Fonstad MA, Marcus WA. 2010. High resolution, basin extent observations and implications for

understanding river form and process. *Earth Surface Processes and Landforms* **35**(6), 680-698.

Gimenez R, Marzolff I, Campo MA, Seeger M, Ries JB, Casali J, Alvarez-Mozos J. 2009.

Accuracy of high-resolution photogrammetric measurements of gullies with contrasting

morphology. *Earth Surface Processes and Landforms* **34**(14): 1915-1926.

Hancock G, and Willgoose G. 2001. The production of digital elevation models for experimental

model landscapes. *Earth Surface Processes and Landforms* **26**: 475-490.

Heimsath AM, Farid H. 2002. Hillslope topography from unconstrained photographs.

Mathematical Geology **34**(8): 929-952.

Heimsath AM, Farid H. 2003. "Hillslope topography from unconstrained photographs" by A.M.

Heimsath and Hany Farid - Reply. *Mathematical Geology* **35**(3): 351-352.

Lane SN. 2000. The measurement of river channel morphology using digital photogrammetry.

Photogrammetric Record **16**(96): 937-957.

Lane SN. 2003. Editorial: The generation of high quality topographic data for hydrology and geomorphology: New data sources, new applications and new problems. *Earth Surface Processes and Landforms* **28**(3): 229-230.

Lane SN, Westaway RM, Hicks DM. 2003. Estimation of erosion and deposition volumes in a large, gravel-bed, braided river using synoptic remote sensing. *Earth Surface Processes and Landforms* **28**(3): 249-271.

Lane SN, Widdison PE, Thomas RE, Ashworth PJ, Best JL, Lunt IA, Smith GHS, Simpson CJ. 2010. Quantification of braided river channel change using archival digital image analysis. *Earth Surface Processes and Landforms* **35**(8): 971-985.

Marcus WA, Fonstad MA. 2008. Optical remote mapping of rivers at sub-meter resolutions and basin extents. *Earth Surface Processes and Landforms* **33**, 4-24.

Marzolff I, Poesen J. 2009. The potential of 3D gully monitoring with GIS using high-resolution aerial photography and a digital photogrammetry system. *Geomorphology* **111**(1-2): 48-60.

Rango, A., Laliberte, A., Herrick, J. E., Winters, C., Havstad, K., Steele, C., and Browning, D. 2009. Unmanned aerial vehicle-based remote sensing for rangeland assessment, monitoring, and management. *Journal of Applied Remote Sensing*, **3**. 10.1117/1.3216822

Snavely N. 2008. Scene reconstruction and visualization from internet photo collections. Doctoral Thesis, University of Washington. 192 pp.

Snavely N, Seitz SM, Szeliski R. 2006. Photo tourism: Exploring photo collections in 3D. *ACM Transactions on Graphics* **25**(3): 835-846.

Snavely N, Seitz SM, Szeliski R. 2008. Modeling the world from internet photo collections. *International Journal of Computer Vision* **80**(12): 189-210.

Templeton RC, Vivone ER, Mendez-Barroso LA, Rango A, Laliberte A, Saripalli, S. 2010. Emerging technologies for ecohydrological studies during the North American monsoon in a Chihuahuan desert watershed. Poster H53B-1014. 2010 American Geophysical Conference annual conference, San Francisco, USA.

Verhoeven GJJ. 2009. Providing an archaeological bird's-eye view – an overall picture of ground-based means to execute low-altitude aerial photography (LAAP) in archaeology. *Archaeological Prospection* **16**(4), 233-249.

Verhoeven GJJ, Loenders J, Vermeulen F, Docter R. 2009. Helikite aerial photography – a versatile means of unmanned, radio controlled, low-altitude aerial archaeology. *Archaeological Prospection* **16**(2), 125-138.

Vericat D, Brasington J, Wheaton J, Cowie M. 2009. Accuracy assessment of aerial photographs acquired using lighter-than-air blimps: low-cost tools for mapping river corridors. *River Research and Applications* **25**(8), 985-1000.

Welty E, Pfeffer WT, Ahn Y. 2010. Something for everyone: quantifying evolving (glacial) landscapes with your camera. Poster IN33B-1314. 2010 American Geophysical Union annual conference, San Francisco, USA.

Westaway RM, Lane SN, Hicks DM. 2003. Remote survey of large-scale braided, gravel-bed rivers using digital photogrammetry and image analysis. *International Journal of Remote Sensing* **24**(4): 795-815.

Wheaton JM, Brasington J, Darby SE, Sear DA. 2010. Accounting for uncertainty in DEMs from repeat topographic surveys: improved sediment budgets. *Earth Surface Processes and Landforms* **35**(2): 136-156.

Wolf PR, Dewitt BA. 2000. *Elements of Photogrammetry with Applications in GIS (3rd Edition)*. McGraw-Hill Professional Co., 608 pp.

Table 1: Comparisons of independent GPS-observations with projected SfM and LiDAR datasets.

Dataset (n=15)	Mean Δ* X (StDev)	Mean Δ Y (StDev)	Mean Δ Z (StDev)	Mean Distance to GPS point** (StDev)
SfM - GPS	-0.03 m (0.19)	0.05 m (0.26)	0.07 m (0.15)	0.21 m (0.25)
LiDAR - GPS	-0.04 m (0.32)	-0.03 (0.39)	0.51 m (0.18)	0.44 m (0.21)

* Mean Δ values were calculated by subtracting the GPS values from the dataset of comparison and averaging the entire dataset.

** Point comparisons were obtained by extracting the nearest spatial neighbor for the 15 GPS validation points.

LIST OF FIGURES

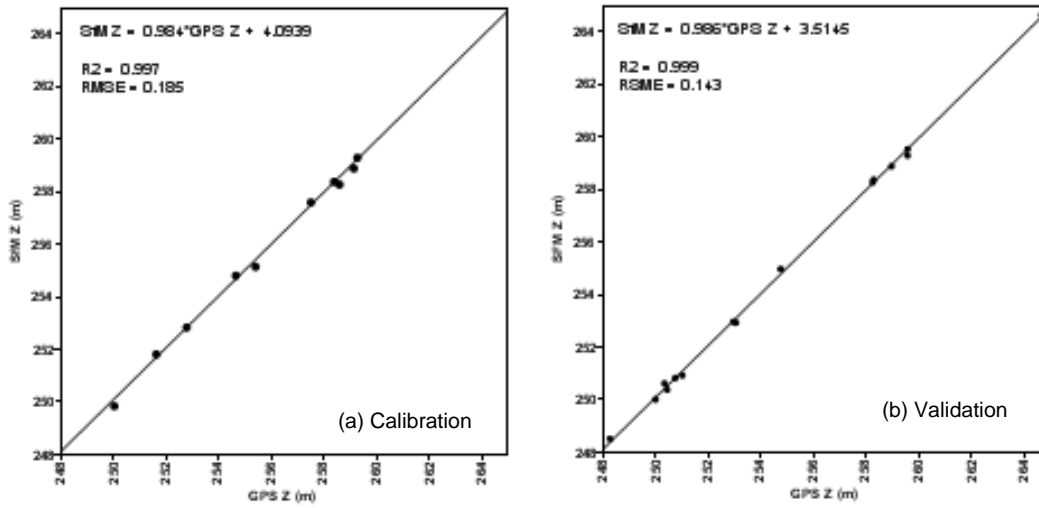Figure 1. Overview of study area and GPS data collection locations.

Figure 2: Calibration (a) and validation (b) plots of the fit between projected SfM Z values and GPS observed orthometric height.
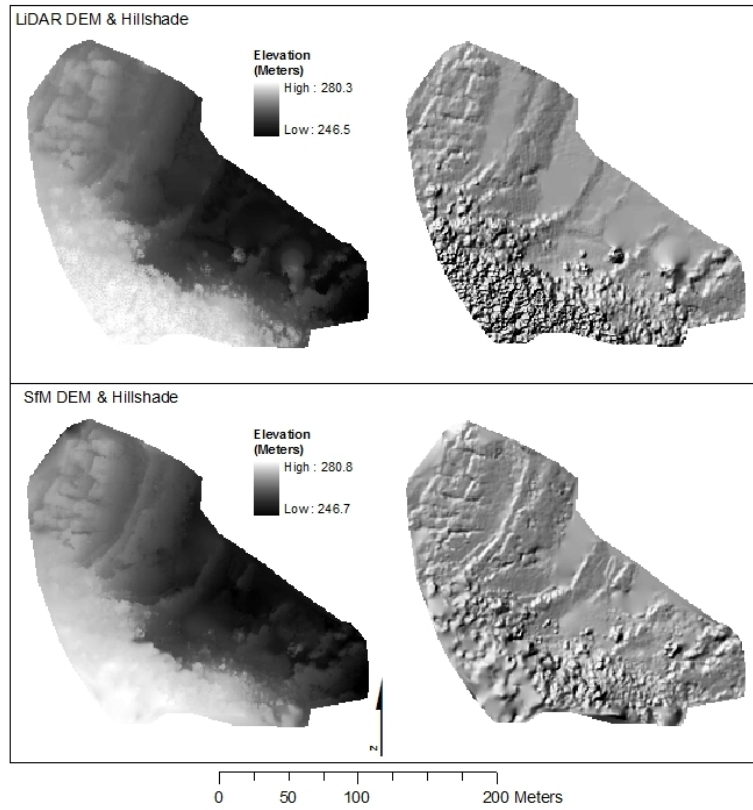
Figure 3. Elevation surfaces from both the LiDAR and SfM datasets. The two hillshade images are presented for improved visual interpretation.
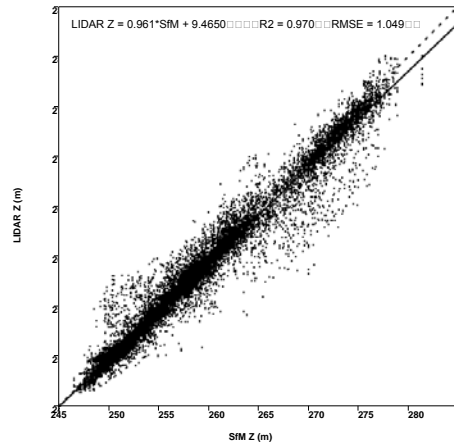
Figure 4. Scatterplot of LiDAR elevations vs. SfM elevations. The dashed line represents the 1:1 relationship. The solid line is the best-fit least squares regression line between the SfM elevations and those from LiDAR.
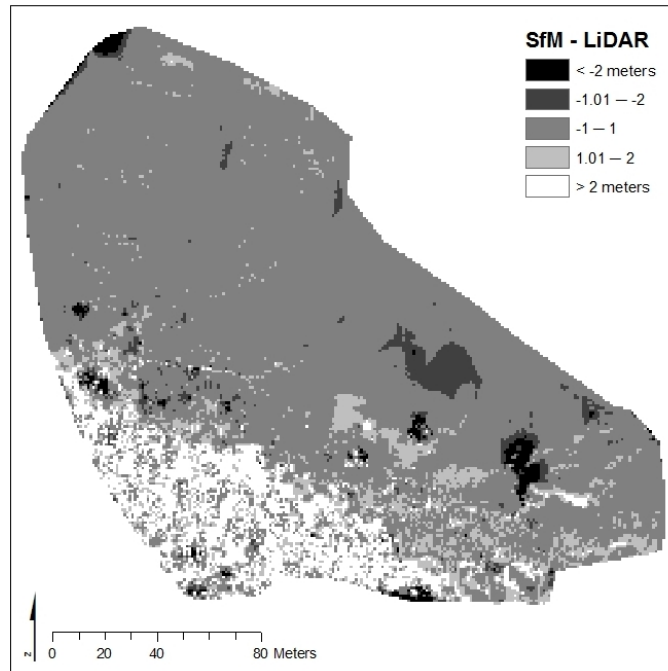
Figure 5. Distribution of SfM and LiDAR elevation differences.

Figure 6. A close-up image taken with the helikite (left) and the same image overlaid with red topographic points derived using SfM (right). Even some submerged areas produce valid topographic points, as long as they are clear and have some spatial texture. In these frames such points are red, but cover the greenish-colored submerged bed.

Figure 7. Oblique view of a section of the Pedernales Falls research area georeferenced point cloud. The length of this point cloud area is approximately 200 meters. The large linear black areas are deep water.